Effect of Trifluoroethanol on Protein Secondary Structure: An NMR and CD Study Using a Synthetic Actin Peptide†

F. D. Sönnichsen, J. E. Van Eyk, R. S. Hodges, and B. D. Sykes*

MRC Group in Protein Structure and Function and Department of Biochemistry, University of Alberta, Edmonton, Alberta T6G 2H7, Canada

Received April 16, 1992; Revised Manuscript Received June 10, 1992

ABSTRACT: The structure of a synthetic peptide comprising the 28 amino-terminal residues of actin has been examined by ^{1}H-NMR and CD spectroscopy. The peptide is largely unstructured and flexible in solution but becomes increasingly structured at higher trifluoroethanol (TFE) concentrations. As judged by CD with the use of two additional peptides (actin 1–20 and actin 18–28), TFE induces formation of up to 48% helical content within residues 1–20, while residues 21–28 exhibit no helical propensity. Similar results were obtained by using NMR-derived distance information in restrained molecular dynamics calculations. The calculated structure of actin 1–28 peptide in 80% TFE is well defined for the first 23 residues with a backbone root mean square deviation of 0.5 Å. Two helices are formed from residues 4–13 and 16–20, and a β-turn is formed from residues 13–16. The N-terminal residues 1–3 exhibit increased flexibility and a helix-like conformation while the C-terminal residues 21–28 show no regular secondary structure. These results are compared with the predicted secondary structure and the structure of the corresponding sequence in the crystal structure of actin [Kabsch et al. (1990) *Nature 347*, 37–44]. The significance of the TFE-induced peptide structure is discussed.

Trifluoroethanol (TFE)[1] has been widely used as a structure-inducing cosolvent since the initial works on the RNase S-peptide (Tamburro et al., 1968) and on oligopeptides (Goodman et al., 1971). It enhances the solution structure of smaller protein fragments like the RNase S- and C-peptides (Nelson & Kallenbach, 1989), the first peptides shown to exhibit a stable protein-like conformation in solution (Bierzinsky et al., 1982; Kim et al., 1982). Additionally, TFE can induce the formation of stable conformations in peptides which are otherwise unstructured in aqueous solution (Greff et al., 1976a; Lau et al., 1984a; Marion et al., 1988; Bruch & Gierasch, 1990; Yamamoto et al., 1990). Several properties have been suggested to be responsible for the observed secondary structure stabilization. The dielectric constant of TFE more closely approximates that of the interior of proteins. It is about one-third that of water, which should strengthen interactions between charged groups. However, Nelson and Kallenbach (1986) demonstrated that the magnitude of the charge group effect is not affected by the TFE concentration. Differences in the solvent acidity and basicity between TFE and water are proposed to change the relative stability of hydrogen bonds. This was probed by NMR (Llinas & Klein, 1975); the results indicate that the dominant effect of TFE is caused by its significantly weaker basicity. Hydrogen bonding of amide protons to the solvent is decreased, which strengthens intramolecular hydrogen bonds and therefore stabilizes secondary structure (Nelson & Kallenbach, 1986). Futhermore, TFE is a less polar or more hydrophobic solvent. It interrupts hydrophobic interactions and can act as a denaturant of tertiary and quaternary structure (Lau et al., 1984b).

The vast majority of investigations used peptides and protein fragments corresponding to helical regions in proteins and established a strong correlation between the TFE-induced structure and the protein structure (Moroder et al., 1975; Lu et al., 1984; Leist & Thomas, 1984; Jimenez et al., 1987; Dyson et al., 1988; Peña et al., 1989; Segawa et al., 1991). TFE is therefore known as a helix-inducing solvent. However, a systematic study with fragments of the all-helix protein bovine growth hormone (Lehrman et al., 1990) found a poor correlation between the TFE-induced structure and the structure of the corresponding protein region. The weak correlation was caused by the significantly lower helical content observed by CD in the peptide fragments as compared to the crystal structure.

Although TFE is often assumed to stabilize native protein-like structures in peptides in general, this is not widely accepted since little is known about the effect of TFE on other secondary structure elements. We have encountered only two cases were TFE is assumed to stabilize β-turn conformations (Cann et al., 1987; Siligardi et al., 1987). The effect on β-sheet structures is less clear; it seems to depend on the TFE concentration as well as the sheet length. Studies with homooligopeptides, host guest peptides (Goodman et al., 1971; Maser et al., 1984; Mutter & Altmann, 1985), and fragments of angiotensin II (Greff et al., 1976b) have shown the existence of β-sheet structures over wide concentration ranges of TFE up to pure TFE solutions. A prerequisite for this β-sheet formation was that the peptide exceeded the critical chain length of 7–9 residues. Although CD studies with fragments of human C3a (Lu et al., 1984) and myelin basic protein (Martenson et al., 1985) indicate that TFE might actually induce β-sheet formation, generally, TFE seems to have a destabilizing effect and induces β-sheet → helix transformations, at least at higher TFE concentrations (Reutimann et

† This work was supported by research grants from the Medical Research Council of Canada and an Alberta Heritage Foundation for Medical Research Fellowship (F.D.S.).

[1] Abbreviations: 1D, one dimensional; 2D, two dimensional; BHA, benzhydrylamine; CD, circular dichroism; DNase, deoxyribonuclease; DQF-COSY, double quantum filtered correlation spectroscopy; DSS, 4,4-dimethyl-4-silapentane-1-sulfonate; HMM, heavy meromyosin; HPLC, high-performance liquid chromatography; NOE, nuclear Overhauser enhancement; NOESY, nuclear Overhauser enhancement spectroscopy; NMR, nuclear magnetic resonance; RMD; restrained molecular dynamics; rms, root mean square; RNase, ribonuclease; S1, myosin subfragment 1; TFA, trifluoroacetic acid; TFE, 2,2,2-trifluoroethanol; TOCSY, total correlation spectroscopy.

0006-2960/92/0431-8790$03.00/0

al., 1981; Stone et al., 1985; Martenson et al., 1985).

We have been interested in synthetic peptides comprising the N-terminal residues of actin for some time. Several investigations indicate the involvement of the amino-terminal residues of actin in actin–troponin and actin–myosin interactions, the basis for regulation and force development in muscle. These peptides, in particular actin 1–28 peptide, bind to troponin, myosin S1, and HMM as well as mimic the biological activity of actin (Van Eyk & Hodges, 1991; Van Eyk et al., 1991; J. E. Van Eyk and R. S. Hodges, unpublished results). As judged by NMR, the peptide is very flexible in solution and exhibits no preferred conformation. In contrast, this portion of the actin sequence is well structured in the crystal structure of actin–DNase complex (Kabsch et al., 1990). All major types of secondary structure occur in the first 28 residues; two strands of antiparallel β-sheet, one β-turn, and two coil regions (a loop and a helix-like sequence). Therefore, peptides of the N-terminus of actin appeared to be ideal to delineate the effect of TFE on different inherent secondary structure elements in small protein fragments and to compare the TFE-induced structure to the structure of the corresponding region in the protein.

EXPERIMENTAL PROCEDURES

Materials. Copolystyrene (1% divinylbenzene) benzhydrylamine hydrochloride resin was purchased from Institute Armand Frappier (Laval, Quebec, Canada). Protected amino acid derivatives were obtained either from Bachem Fine Chemicals (Torrance, LA) or Institute Armand Frappier. 2,2,2-Trifluoroethanol-d_3 was purchased from Cambridge Isotope Laboratories (Cambridge, MA). All other materials were of analytical grade and as described by Hodges et al. (1988b).

Peptide Synthesis and Purification. The peptides actin 1–28 (Ac-D-E-D-E-T-T-A-L-V-A-D-N-G-S-G-L-V-K-A-G-F-A-G-D-D-A-P-R-amide), actin 1–20 (Ac-D-E-D-E-T-T-A-L-V-A-D-N-G-S-G-L-V-K-A-G-amide), and actin 18–28 (Ac-K-A-G-F-A-G-D-D-A-P-R-amide) were synthesized using standard procedures as described by Hodges et al. (1988b) for solid-phase peptide synthesis (Erickson & Merrifield, 1976) on an Applied Biosystems 430A peptide synthesizer (Foster City, CA). All amino acids were protected at their α-amino group with the Boc group, and the side-chain protecting groups were used as follows: Tosyl (Arg), benzyl (Asp, Glu), benzoyl (Ser, Thr), and 2-chlorobenzyloxycarbonyl (Lys). The first residues were coupled directly to the BHA resin, which yields a neutral, amidated carboxy-terminus after HF cleavage. The N-terminus was acetylated with a mixture of acetic anhydride/toluene/pyridine (1:3:3, v/v/v) to obtain a neutral N-terminal residue, which is acetylated as found in the native actin sequence. Cys at position 10 in the native actin sequence was substituted with an alanine in the synthetic peptide. This change eliminated any problems related to the oxidation of the cysteine.

The crude peptides were purified on a HPLC system comprised of a Spectra Physics SP8700 solvent delivery system, Kratos SF7697 detector, and an analytical reversed-phase column (4.6 mm i.d. × 220 mm) (Aquapore RP-300, 300-Å pore size and 7.5-μm particle size, Pierce Chemicals, CA). A linear AB gradient of 0.1% B min^{-1} at 1 mL min^{-1} was used, in which solvent A was 0.05% aqueous TFA and solvent B was 0.05% TFA in acetonitrile. The sample loads varied between 20 and 50 mg per run (Mant et al., 1987; Hodges et al., 1988a, 1991), and 1-mL fractions were collected. In order to identify fractions containing the desired peptide, analytical runs of the various fractions were carried out using the HPLC system described above with a linear AB gradient rate of 1% B/min. The fractions containing the pure peptide were pooled and lyophilized. The peptides were characterized by amino acid analysis on a Beckman System 6300 amino acid analyzer (Beckman Instruments, Fullerton, CA); the correct primary ion molecular weights were confirmed by plasma desorption time of flight mass spectrometry using a BioIon-20 spectrometer (Applied Biosystems Inc., Foster City, CA). The results were consistent with the sequence of each peptide.

CD Experiments. Circular dichroism spectra were recorded at temperatures between 5 and 35 °C on a Jasco J-500 C spectropolarimeter (Jasco, Eaton, MD) attached to a Jasco DP-500/PS 2 system via Jasco IF-500 II interface. A Lauda (Model RMS) water bath (Brinkman Instruments, Rexdale, Ontario, Canada) was used to control the temperature of the cell. The instrument was routinely calibrated with an aqueous solution of recrystallized *d*-10-camphorsulfonic acid. Ellipticity is reported as mean residue molar ellipticity. The α-helicity was calculated by using the mean residue ellipticity at 220 nm [θ_{220}] and the equation of Chen et al. (1974) for the chain length dependence of helices:

$$[\theta]_\lambda = (f_H - ik/N)\,[\theta]_{H\lambda\infty}$$

where $[\theta]_\lambda$ is the observed mean residue ellipticity at wavelength λ, $[\theta]_{H\infty}$ is the maximum mean residue ellipticity of a helix of infinite length (Chang et al., 1978), f_H is the fraction of helix in the molecule, i is the number of helical segments, N is the total number of residues, and k is a wavelength-dependent constant (2.6 at 220 nm). Contributions from β-sheet or random coil were omitted, because no indications for the existence of β-sheet structure were found and the contribution of random coil structure to the [θ_{220}] value was empirically determined in 8 M urea to be negligible. The expected values of the mean residue ellipticity for 100% helicity of peptides of the chain lengths 28, 20, and 11 residues were determined to −32930, −31580, and −27720 deg·cm^2/dmol, respectively.

The peptides were dissolved in a buffer solution containing 20 mM potassium phosphate and 50 mM KCl at pH = 5.5–5.8. Peptide concentrations were in the range of 0.2–0.8 mg/mL as determined by amino acid analysis (0.05–0.7 mM). Changes in either salt or peptide concentration did not affect the resulting CD spectra.

Proton NMR Experiments. For measurement of NMR spectra the actin 1–28 peptide was dissolved in aqueous buffer at pH = 4.05 before TFE-d_3 was added to yield a 50% or 80% aqueous TFE solution. The sample volume was 600 μL, and final salt concentrations were 50 mM KCl and 50 mM potassium phosphate. The ^{1}H-NMR spectra were acquired at 5 °C on a Varian VXR-500 spectrometer. A spectral width of 5500 Hz, a low-pass filter of ±3100 Hz, and a pulse width of 13 μs (≅90°) were used. Saturation of the solvent protons was accomplished by a 2.5-s presaturation pulse. One-dimensional spectra were acquired using 512 transients and 21 888 data points, which were zero filled to 65 536 data points. For 2D spectra 2048 complex data points, 32 transients, and 256 increments were acquired and zero filled to 4K × 4K data points. All chemical shifts were referenced to the methyl resonance of 4,4-dimethyl-4-silapentane-1-sulfonate (DSS, 0 ppm).

Resonances were assigned to residue type by DQF-COSY spectra (Piantini et al., 1982; Rance et al., 1983) and TOCSY spectra (Braunschweiler & Ernst, 1983; Davis & Bax, 1985). Sequential assignments were made using NOESY spectra (Jeener et al., 1979) and standard procedures (Wüthrich, 1986)

and by comparison with the spectra obtained from actin 1–28 peptide in aqueous solution (Van Eyk et al., 1991). Assigned cross-peaks were converted into distance restraints using the cross-peak between Phe β- and ortho-protons for calibration (2.5 Å). The intensity of cross-peaks involving amide protons were corrected for the proton/deuterium ratio of the solvent. The cross-peak intensity was classified into strong, medium, or weak for which distance restraints of 1.8–2.7, 1.8–3.3, or 2.3–5 Å were used, respectively. Pseudoatom corrections were used for methylene and methyl groups, an additional correction of 0.5 Å was used for methyl groups.

Restrained Molecular Dynamics Calculations. The structures of actin 1–28 peptide were calculated by using the constant valence force field (CVFF) included in the Biosym-Software (INSIGHT II 2.0.0, DISCOVER 2.71) (San Diego, CA) on a Silicon Graphics Personal IRIS 4D/35.

The distance information was included in the total energy expression using skewed biharmonic functions for the lower and upper boundaries for proton–proton distances, which were determined as described above. Additional torsional restraints of identical form were applied to maintain trans-geometry and planarity for the peptide bond throughout the calculations. Coulomb interactions and cross terms were excluded from the calculation, and harmonic bond potentials were used. A cutoff of 10 Å with a switching function from 1 at 8 Å to 0 at 9.5 Å limited the number of calculated nonbonded interactions to accelerate the calculation. The procedure used here is similar to the calculation described by Gippert et al. (1990). The force constant for nonbonded interactions was scaled to 1/100 of the default value. The starting coordinates were minimized using 50 steps of steepest descent minimization followed by 600 fs of molecular dynamics calculation at 1200 K with a step size of 1 fs, where 100 fs were performed with direct velocity scaling to maintain the target temperature ±10 K and then with weak coupling to an external temperature bath. The distance and torsional restraints were then included with initial force constants of 0.02 kcal/Å^2 and 0.04 kcal/rad^2, respectively. After initialization for 100 fs, the dynamics calculation was repeated for blocks of 500 fs, until the remaining potential energy due to distance and angle forcing fell below 120 or 150 kcal/mol. Usually, 1–4 repetitions at each force constant were sufficient. Then the force constants were doubled, and the dynamics calculation was continued. The force constant for nonbonded interactions was scaled up to 1/10 of the default value at a NOE force constant of 5 kcal/mol and to the default value when a NOE constant of 20 kcal/mol was reached. Reaching the final NOE force constant of 38–40 kcal/Å^2, 2 ps of dynamics calculation were performed. The following annealing or cooling procedure is significantly different from Gippert et al. (1990) and was designed to allow an initially slow and increasingly faster cooling of the dynamics calculation down to room temperature. DISCOVER uses an algorithm which removes kinetic energy in an exponential fashion controlled by a time constant τ. Due to the partitioning between kinetic and potential energy, the actual time constant for the temperature decay between initial or starting temperature and target temperature is 2 τ. The default value (used throughout the calculations above) for the thermal coupling between kinetic energy and temperature is 0.1 ps. For the cooling procedure, a time constant of 1 ps was used to slow down the temperature change. Since a direct use of 300 K as the target temperature (T) would have resulted in an initially fast cooling, the temperature was decreased in steps of 50 °C every 1500 fs to 1000 K. Subsequently T was decreased by 100 K every 500 fs to 700 K. τ was then changed to 0.5 ps, and T was changed to 500 K for 500 fs, before the cooling concludes with a return to τ of 0.1 fs and T of 300 K. The latter changes were made to speed up the cooling at lower temperature, thus significantly shortening the cooling procedure with no effect on the final structure. The calculation was continued at 300 K for 3 ps to reach an equilibrium at room temperature. Finally, the structure was minimized (200 steps steepest descent, 2000 steps conjugate gradient). This procedure was repeated 50 times using different random velocity assignments; 25 times using helical and 25 times using extended starting coordinates; 38 structures were obtained showing similar fold, no violations of distance restraints (>0.4 Å) and reasonable nonbonded interaction energy. These structures were superimposed, a mean structure as well as rmsd comparisons calculated with programs written by T. Jellard, University of Alberta. The mean structure was finally minimized (100 steps steepest descent, 1000 steps conjugate gradient).

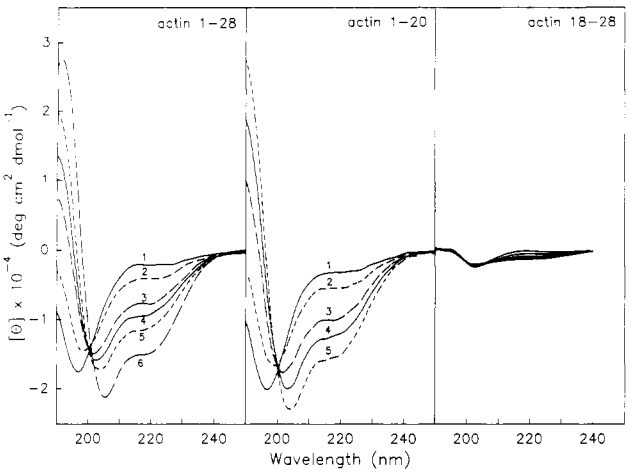

FIGURE 1: Low-ultraviolet CD spectra of actin 1–28, actin 1–20, and actin 18–20 peptides at various concentrations of TFE and buffer solution containing 50 mM KCl and 20 mM K_2HPO_4, pH = 5.54. (A) Actin 1–28; (B) actin 1–20; (C) actin 18–28. Curves 1–5 represent 0%, 20%, 40%, 60%, and 80% TFE (v/v) at 20 °C, respectively. Curve 6 shows actin 1–28 peptide in 80% TFE at 5 °C.

Secondary Structure Predictions. Secondary structure predictions have been performed by using the methods of Chou and Fasman (1978), Garnier et al. (1978), and Eisenberg et al. (1984), which were available as part of the software package SEQSEE, written by R. Boyko and D. Wishart, University of Alberta. The parameter sets were updated using a database of 245 protein structures (D. S. Wishart, unpublished results). The propensities for coil, α-helix, and β-sheet structure were determined, but only the largest propensity is presented for each residue.

RESULTS

CD Experiments. Figure 1 shows the CD spectra obtained for the peptides actin 1–28, actin 1–20, and actin 18–28 at different TFE concentrations. The spectra of actin 18–28 are hardly affected by the change of solvent, showing only a very small change in ellipticity upon TFE addition. These CD spectra are characteristic for random coil conformations; no significant content of α-helix or β-sheet can be detected. The spectra of actin 1–20 and actin 1–28 are very similar to each other. The shape of the curves is increasingly characteristic of α-helical secondary structure. The minimum absorption peak ($\pi\pi^*$-transition) shifts from 197 to 204 nm and the negative ellipticity at 220 nm ($n\pi^*$-transition) increases with the TFE concentration. An isodichroic point is indicative of

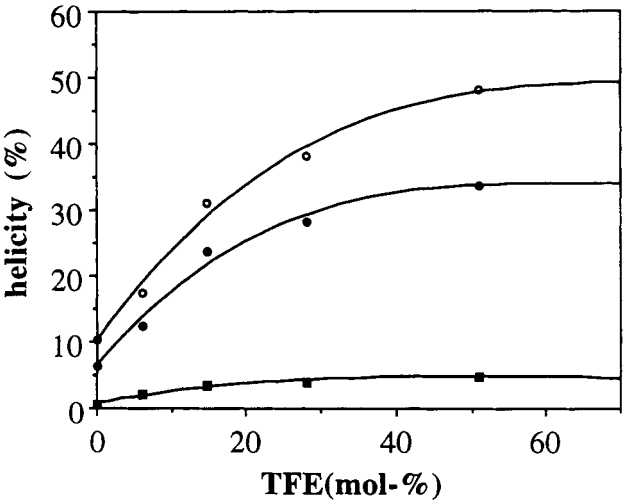

FIGURE 2: α-Helicity calculated from CD (θ_{220}) for actin peptides as a function of TFE: (○) actin 1–20; (●) actin 1–28; (■) actin 18–28. Conditions are as described in Figure 1.

an equilibrium betewen two conformational states, random coil and α-helix. The calculated helicity using the mean residue ellipticity at 220 nm is small for both peptides in water, being 7% for actin 1–28 and 11% for actin 1–20. The helicity increases steadily with the TFE concentration showing a saturating curve for the helicity versus TFE concentration in mol % (Figure 2). The shape of the curve can be interpreted in terms of a two-state transition. The helicity at 80% TFE (v/v) was calculated to be 34% for actin 1–28 peptide and 48% for actin 1–20 peptide at 20 °C. This corresponds to an estimate of 10 residues being involved in α-helical structures, an identical result for both peptides. In conjunction with the observed lack of helicity for actin 18–28 this result indicates that all helix-forming residues are located in the first 20 residues of the sequence. The negative ellipticity increases with decreasing temperature, and the helical content for actin 1–28 peptide was determined to be 45% at 5 °C.

NMR Experiments. The NMR spectra of actin 1–28 peptide obtained at two different TFE concentrations (50% and 80%) were essentially identical except for a higher number of NOE cross-peaks observed in the NOESY spectra in 80% TFE/H_2O (v/v). Since the CD spectra did not indicate major conformational changes between these concentrations, we primarily used data taken at 80% TFE (Figure 3). The chemical shifts of the proton resonances (δ_{TFE}) are given in Table I. Compared to the proton chemical shifts of actin 1–28 in aqueous solution (δ_{H2O}), significant shifts ($\Delta\delta = \delta_{TFE} - \delta_{H2O}$) are observed for αCH-resonances (Figure 4). Also presented in Figure 4 is a similar comparison with average chemical shifts expected for residues in random coil ($\Delta\delta = \delta_{TFE} - \delta_{RC}$) as determined by Wishart et al. (1991). The curves are smoothed, i.e., each point is averaged with its ±1 neighbors to average out local effects (Pastore & Saudek, 1990). Both curves are basically similar, because the chemical shifts determined for actin 1–28 in aqueous solution are close to the random coil value as expected for a flexible peptide. The observed relative shifts are therefore indicative of structural changes induced by addition of TFE to the solvent. Applying the criteria for secondary structure determination based on chemical shifts (Wishart et al., 1991), adjacent αCH-protons from residue 3-to residue 11 show upfield shifts upon TFE addition, indicative of the formation of a helix. A second helix might exist between residues 16 and 19 or 17 and 20, where three adjacent upfield shifted αCH-protons are observed. The regions from 20 to 23 and from 24 to 28 show

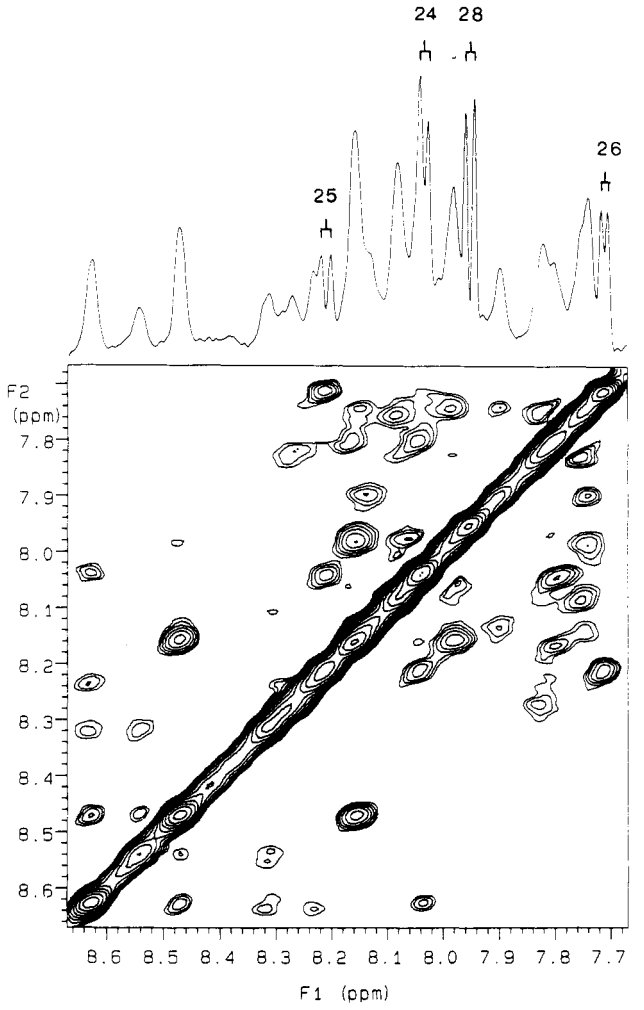

FIGURE 3: Amide region of the ^1H 2D NOESY NMR spectrum and 1D ^1H-NMR spectrum of actin 1–28 at 80% TFE (v/v) at 5 °C. Some resonance assignments are indicated for more flexible C-terminal residues of the peptide.

no shifts or slight downfield shifts of αCH-resonances, respectively. This indicates that TFE does not stabilize a specific conformation in the former region, but could stabilize a more extended conformation in the latter region. In the 1D spectrum (Figure 3), four amide resonances are easily detected having a narrower line width and a larger $J_{N\alpha}$ coupling constant, indicative of a more flexible, extended region from 24 to 28.

Proton–proton connectivities as determined from NOESY spectra are given in Figure 5. Two regions of the peptide are well characterized showing $d_{\alpha N}$ (i, i+3) NOEs, continuous stretches of d_{NN} (i, i+1) NOEs, and decreased $d_{\alpha N}$ (i, i+1) connectivities. These establish helix formation from residue 4 to residue 12 and give further support for a second helix of approximately 1.5 turns from residue 16 to residue 20. The N-terminal helix could also extend into residues 1–4. Though there were fewer cross-peaks and no $d_{\alpha N}$ (i, i+3) cross-peaks observed, the existence of d_{NN} sequential connectivities from 1 to 4 support a loosened helical structure. No significant or characteristic NOE cross-peak patterns were observed for the remaining regions of the peptide, residues 13–15 and 20–28. Both regions show only a small number of interresidue, primarily sequential connectivities. This might be expected for residues 13–15, since the number of protons is small due to the sequence G-S-G, while the lack of structural information for residues 21–28 agrees with the higher flexibility of this region expected from the CD and 1D NMR results.

Table I: Proton Chemical Shifts of Actin 1–28 Peptide[a]

no.	residue	NH	αCH	βCH	γCH	others
	acetyl		2.11			
1	Asp	8.03	4.87	3.00, 3.00		
2	Glu	8.62	4.32	2.20, 2.17	2.58, 2.58	
3	Asp	8.46	4.62	3.00, 3.00		
4	Glu	8.16	4.23	2.21, 2.21	2.57, 2.57	
5	Thr	8.12	4.04	4.32	1.33	
6	Thr	7.89	3.97	4.32	1.32	
7	Ala	7.74	4.13	1.55		
8	Leu	7.98	4.20	1.99, 1.71	1.85	δCH 0.98, 0.98
9	Val	8.14	3.80	2.26	1.13, 1.02	
10	Ala	8.46	4.22	1.54		
11	Asp	8.53	4.66	3.12, 3.03		
12	Asn	8.31	4.70	3.00, 2.94		NH 7.63, 6.60
13	Gly	8.63	4.04, 4.04			
14	Ser	8.23	4.30	4.08, 4.08		
15	Gly	8.27	3.97, 3.96			
16	Leu	7.82	4.28	1.93, 1.66	1.77	δCH 0.99, 0.92
17	Val	7.74	3.84	2.23	1.09, 1.02	
18	Lys	8.07	4.17	1.98, 1.67	1.51, 1.51	δCH 1.75, 1.75, εH 3.01, ζH 7.59
19	Ala	8.07	4.26	1.54		
20	Gly	8.05	3.96, 3.96			
21	Phe	7.97	4.63	3.28, 3.17		aromatic CH 7.35
22	Ala	8.15	4.28	1.50		
23	Gly	7.79	3.96, 3.94			
24	Asp	8.04	4.76	3.01, 2.99		
25	Asp	8.20	4.83	2.98, 2.90		
26	Ala	7.71	4.59	1.44		
27	Pro		4.45	2.32, 1.96	2.13, 2.06	δCH 3.81, 3.64
28	Arg	7.94	4.42	1.95, 1.81	1.74, 1.74	δCH 3.24, 3.24, εCH 7.11, ζCH
	amide	7.35, 6.73				6.76, 6.39

[a] The chemical shifts are given in ppm and are referenced to DSS (0 ppm).

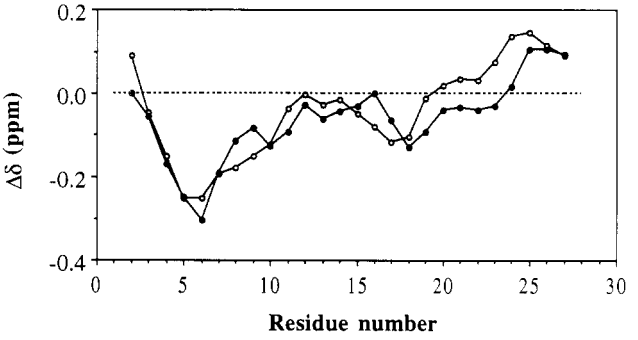

FIGURE 4: Difference between ^{1}H-NMR chemical shifts of αCH-protons of actin 1–28 in TFE and (○) actin 1–28 in aqueous solution ($\Delta\delta = \delta_{TFE} - \delta_{H2O}$) and (●) random coil values (Wishart et al., 1991) ($\Delta\delta = \delta_{TFE} - \delta_{RC}$) as a function of residue number. The graph is smoothed by averaging the value at each point with its ±1 neighbors.

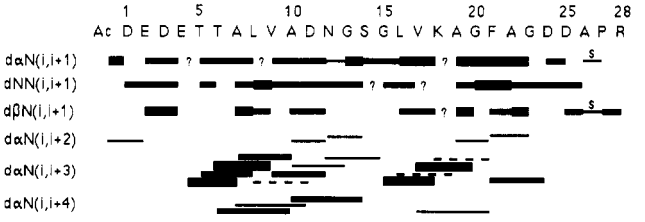

FIGURE 5: Summary of ^{1}H–^{1}H NOE connectivities for actin 1–28 in 80% TFE (v/v). The intensity of NOE cross-peaks is indicated by the thickness of the lines, grouped into strong, medium, and weak. Overlapping and therefore ambiguous cross-peaks are indicated by a ? or a dashed line. Connectivities involving the P^{27} δCH are marked with a letter indicating their size.

In the NOESY spectra 250 NOE cross-peaks were assigned; an average of more than 10 connectivities per residue for the first 20 residues of the peptide. This unusually high number for a peptide allowed us to determine the structure of the peptide using the NOE-derived distance information in restrained molecular dynamics calculations to support the qualitative interpretation of the CD and NMR results and possibly obtain more information about the nonhelical regions of the peptide. The calculations were not expected to yield a very accurate well-defined 3D structure for the following reasons. The current procedures for determining the 3D structure by NMR are well suited for proteins which have only one stable preferred conformation. Applying the same procedures to peptides is difficult, since they are usually more flexible and may have more than one preferred conformation. Therefore, the data acquired by NMR will be an average of all the conformations existing in the time period of acquisition, which is in the range of seconds. Consequently, calculations using NOE-derived distance restraints will yield an average structure between the existing conformations, unless the flexibility is taken into account. This might be accomplished in the future by the use of time-averaged NOE restraints (Torda et al., 1989, 1990) or by averaging over different conformer populations (Landis & Allured, 1991).

In this example, the actin 1–28 peptide gives no indication of conformational flexibility except for the C-terminal part of the peptide. We therefore felt safe in using the standard procedure, allowing for some conformational flexibility by using only loose classifications of distance restraints and pseudoatom corrections to delineate the secondary structure of the peptide. We calculated 38 independent structures of identical global fold starting from either helical or extended coordinates using different random assignments of initial velocities. A superposition best fitting residues 0–23 is presented in Figure 6. The central part of the peptide (from residue 3–20) is well defined. The structures are more flexible at the first 3 N-terminal residues and from residue 20–28 (Figure 6). In agreement with the 1D spectra and the lack of NOE information, the C-terminal region of the peptide exhibits no conformational preferences. The rms comparisons were therefore calculated from residue 0 to residue 23, showing a well-defined structure in this region with an average rmsd

FIGURE 6: Superposition of the backbone (N, αC, C) atoms of 38 structures obtained from restrained molecular dynamics calculations. The structures are best fitted to residues 1–23. Only backbone atoms are displayed.

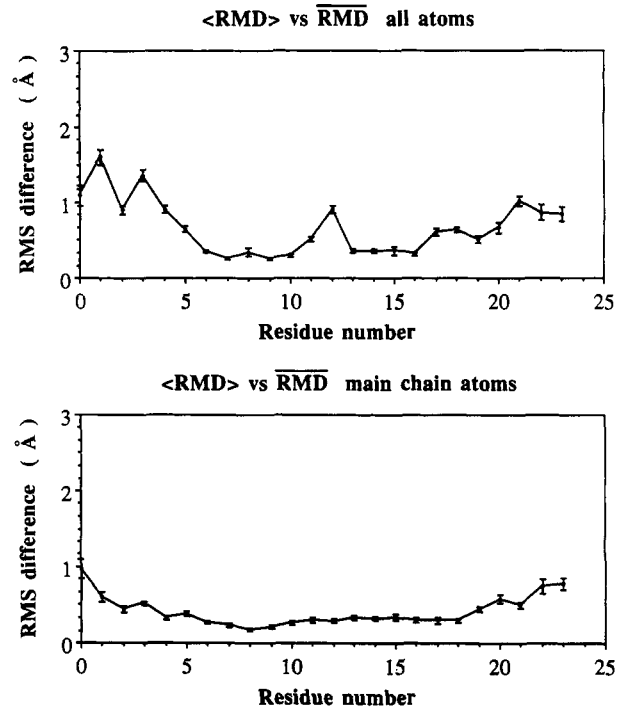

FIGURE 7: Atomic rms distribution of the individual 38 RMD structures best fitted to residues 1–23. The filled circles (●) represent the average rms difference at each residue between the individual structures (<RMD>) and the mean structure ($\overline{RMD}$); the bars represent the standard deviations in these values.

of 0.48 Å (Figure 7). Figure 8 presents the minimized average structure of all 38 structures (from residue 0 to residue 23). A helix extends almost from the N-terminus, well-characterized from residue 4 to residue 13. The calculated average structure establishes 1.5 turns of helix from 16 to 20 as well. Residues 13–16 form a distorted turn with ϕ/ψ angle combinations which do not fit any of the classical β-turn categories.

DISCUSSION

The effect of TFE on the structure of actin 1–28 peptide is profound. It induces a more stable, less flexible conformation in the peptide, which shows no conformational preferences in water alone. Primarily, it induces an increasing amount of α-helical content, which is estimated by CD to be 34% and 45% at a TFE concentration of 80% and temperatures of 20 and 5 °C, respectively. The fact that the maximum stabilizing effect of TFE is reached at this high concentration might indicate that the inherent helical propensity of the actin peptides are small. Peptides with pronounced helical propensity, especially amphipatic peptides, often reach the maximum helical content at much lower TFE concentrations (30–50%) (Lau et al., 1984b; Nelson & Kallenbach, 1989; Lehrmann et al., 1990; Zhou et al., 1990). In these cases, TFE shows a much more cooperative behavior in inducing the formation of helix.

The NMR experiments and molecular dynamics calculations determine a somewhat higher α-helical content, two helices extending from residue 4 to residue 13 and from residue 16 to residue 20, which averages to 54%. Similar discrepancies have been found (Dyson et al., 1988; Bradley et al., 1990). Possible explanations are interconverting helical turns in a predominantly extended structure, minor distortions of the helical structure, interference of tyrosine residues with the CD signal around 220 nm, or the existence of β-turns which have a positive absorption at 224 nm and could reduce the apparent ellipticity at 220 nm. In this case, most of these reasons are not applicable except for the existence of the β-turn, which might contribute to the observed differences in helicity determined by CD and NMR. Another factor could be the clear interruption of the helical content into two separated helices. End effects reduce the maximum predicted ellipticity values for 100% helical peptides. Since the relative contribution of the end effects increases with decreasing peptide length, the equation for chain length dependency was developed (Chen et al., 1974). The formation of two helices in a peptide doubles the contribution of the end effects; we therefore have to account for the number of the helices. If we calculate the helicity with the equation for chain length dependencies assuming two helices of a length of 10 and 5 residues in a 28-residue peptide, we obtain a mean residue ellipticity of −12705 (versus −16075 with the assumption of one helix) as compared to a measured value of −14840 for actin 1–28. In this case, the CD result would actually overestimate the helical content, which can be easily explained with contri-

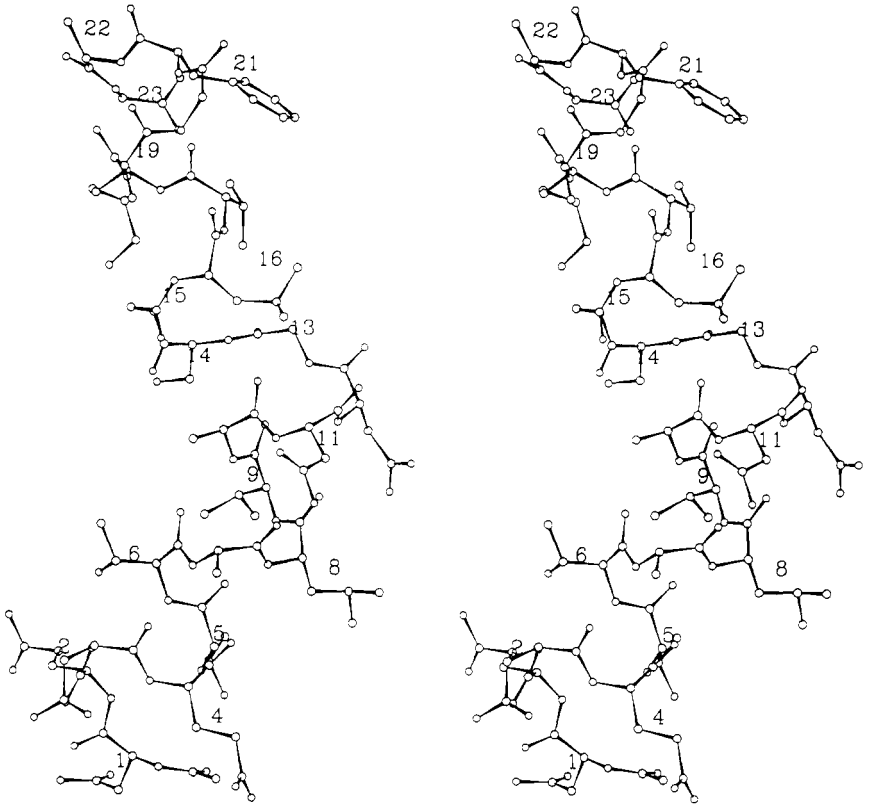

FIGURE 8: Stereoview of the minimized mean structure of all 38 RMD structures.

butions of the helix-like N-terminus to the ellipticity. However, CD and NMR results agree fairly well (within 10%).

Despite the fact that TFE induces the formation of helix in actin 1–28 peptide, it is not simply a helix-enforcing solvent, since not all regions of the peptide become helical. Despite the high concentration of TFE, residues 13–16 stay in a turn conformation. This is surprising since the formation of helix is highly cooperative, but the "helix-stop signal" stays intact (Kim & Baldwin, 1984; Nelson & Kallenbach, 1989). Furthermore, in this case the turn is not only terminating a helix but also interrupting the formation of a possible continuous helix from 4 to 20 as well. This leads to the formation of a short second helix, which seems to be stable in TFE despite its length of only 1.5 turns or 5 residues. The propensity to form a turn seems to persist even under these unusual conformational and environmental circumstances. Another interesting aspect is that Gly-13 and Gly-20 occupy the C-cap positions of the N-terminal and the center helix, respectively. This position is often occupied by glycine residues (Richardson & Richardson, 1988), and TFE does not change this statistically determined positional preference.

Lehrmann et al. (1990) suggested that the TFE-enhanced α-helicity is indicative of the α-helical propensity. Their findings established a strong correlation between TFE-induced helicity and predicted helicity based on amino acid sequence. Table II summarizes the structure predictions for the 28 N-terminal residues of actin using the method of Chou and Fasman (1978) and other methods. All methods predict dominant helical propensity from residue 5 to residue 10. Depending on the method, region 16–20 has either primarily α-helical propensity or β-sheet propensity. However, it should be noted that Table II indicates only the secondary structure with the highest propensity but that for all three methods and for both regions, residue 5–10 as well as 16–20, the propensities for α-helix and β-sheet are very similar. Therefore, the regions

Table II: Secondary Structure Predictions for Actin 1–28 Peptide

				5					10					15					20					25			
Seq	D	E	D	E	T	T	A	L	V	A	D	N	G	S	G	L	V	K	A	G	F	A	G	D	D	A	P	R
CF[a]	C	C	C	C	H	H	H	H	H	H	C	C	C	C	C	C	B	B	B	B	C	C	C	C	C	C	C	C
GOR[b]	C	C	C	H	H	H	H	H	H	H	C	C	C	C	C	C	B	B	B	B	C	C	C	C	C	C	H	H
Mom[c]	C	C	C	C	H	H	H	H	H	H	C	C	C	C	C	H	H	H	H	H	C	C	C	C	C	C	C	C

[a] Chou and Fasman, modified algorithm, Williams et al. (1987). [b] Garnier et al., (1978). [c] Hydrophobic moment, Eisenberg et al. (1984). C = coil, B = β-sheet, H = α-helix.

of actin 1–28 peptide with predicted helical propensity correlate well with the regions found to be helical at higher TFE concentrations. Conversely, regions without helical propensity do not form helices even at high TFE concentrations. Region 21–28 stays nonhelical as well as 13–16, both in agreement with the prediction. Only residues 1–4 seem to form a helix-like structure rather than a regular helix in our results, although the predictions are conclusive in predicting random coil in this area (discussed below).

The strong correlation between TFE-induced and -predicted helicity implies that the statistical analysis of known protein structures (as used in the Chou and Fasman algorithm) has accurately determined residue or sequence-specific conformational preferences. The limited accuracy of structure prediction on the other hand then originates in the optimization of the tertiary structure, which can overrule local secondary structure preferences. Therefore TFE does induce structures which are inherent in the sequence of the peptide or protein fragment, but it does not necessarily simulate a protein-like environment and does not induce a fold which is observed in this sequence in the native, intact protein. This is easily demonstrated by comparison of the TFE-induced structure of actin 1–28 peptide to the structure of this sequence in the native actin as determined by X-ray crystallography of the actin–DNase complex (Kabsch et al., 1990).

The crystal structure defines two β-sheet regions from residue 8 to residue 13 and from residue 16 to residue 21, forming the two antiparallel strands of a five-stranded sheet structure. The antiparallel sheet is facilitated by a β-hairpin turn from 13 to 16. This turn shows unusual ϕ/ψ angle combinations and does not fit into any of the classical turn categories. The N-terminal region is in an irregular but helix-like conformation (residues 1–7), not stabilized by any other part of the protein and fully solvent accessible. Residues 21–28 form a wide loop and are surface accessible as well.

The two helical regions found in the peptide in TFE are mostly part of the β-strands in the intact protein. Therefore, TFE does not induce a protein-like conformation in the peptide, and several explanations are possible. Compared to the protein, the peptide has a greatly reduced propensity to form a β-sheet since it is missing the stabilizing effect of the adjacent strands. TFE does not compensate for this effect. Despite the fact that strengthening of intramolecular hydrogen bonds should promote β-sheet as well as helix formation, TFE at the same time reduces hydrophobic or "neighborhood" interactions. These interactions seem to be more important for the stabilization of β-sheet structures (Mutter et al., 1985). Additionally, the length of the strands seem to be too short to exist in TFE (or water) as judged by the critical length observed for oligopeptides (Muller & Altmann, 1984). Therefore, in peptide regions with both β-sheet and helical propensity, TFE will most likely induce helix formation.

Our studies have not yielded any conformational information on the C-terminus of the peptide, residues 21–28. This region remains flexible and no helix could be observed, which agrees well with the structure of the corresponding region in the protein. Similarly, a turn at position 13–16 is present in both the TFE and crystal structure. The NMR structure in TFE defines the N-terminal residues 1–4 as a loosened, helix-like conformation, which does not disagree with the random coil prediction. While we cannot exclude that the deviations from perfect helical geometry are caused by increased flexibility of these residues, this conformation is similar to the conformation in the protein as well.

While TFE fails to induce a protein-like conformation in the β-sheet regions and enhances α-helicity as predicted, the conformation of regions without helical propensity are similar in the TFE structure and in the protein. Therefore, TFE is not a helix-inducing solvent in the sense that it will induce helix formation independently of the sequence. It is rather a helix-enhancing cosolvent, which stabilizes helices in regions with some α-helical propensity, which in turn can be fairly accurately determined by secondary structure predictions. In this study, similarities between the TFE-induced structure and the structure of the corresponding region in the protein are found for sequences without helical propensity, but there may be little correlation between TFE-induced and native protein-like conformation in general. Conclusions drawn from studies with cosolvents should therefore be evaluated and interpreted carefully and critically. TFE seems to be just another environment to which the flexible peptide can adjust, and the preferred conformation in TFE does not necessarily correlate with the situation in water, in the intact protein, or upon protein–protein interaction.

ACKNOWLEDGMENT

We thank Dr. K. C. Holmes for providing us with the crystal coordinates and Drs. C. M. Kay and D. Wishart for helpful discussions. We are grateful to B. Luty for the acquisition of the CD spectra and to S. Smith for the typing of the manuscript.

REFERENCES

Bierzynski, A., Kim, P. S., & Baldwin, R. L. (1982) *Proc. Natl. Acad. Sci. U.S.A. 79*, 2470–2474.
Bradley, E. K., Thomason, J. F., Cohen, F. E., Kosen, P. A., & Kuntz, I. D. (1990) *J. Mol. Biol. 215*, 607–622.
Braunschweiler, L., & Ernst, R. R. (1983) *J. Magn. Reson. 53*, 521–528.
Bruch, M. D., & Gierasch, L. M. (1990) *J. Biol. Chem. 265*, 3851–3858.
Cann, J. R., London, R. E., Unkefer, C. J., Vavrek, R. J., & Stewart, J. M. (1987) *Int. J. Peptide Protein Res. 29*, 486–496.
Chang, C. T., Wu, C. S. C., & Yang, J. T. (1978) *Anal. Biochem. 91*, 13–31.
Chen, Y. H., Yang, T. Y., & Chau, K. M. (1974) *Biochemistry 13*, 3350–3359.
Chou, P. Y., & Fasman, G. D. (1978) *Annu. Rev. Biochem. 47*, 251–276.
Davis, D. G., & Bax, A. (1985) *J. Am. Chem. Soc. 107*, 2821–2822.
Dyson, H. J., Rance, M., Houghten, R. A., Wright, P. E., & Lerner, R. A. (1988) *J. Mol. Biol. 201*, 201–217.
Eisenberg, D., Weiss, R. M., & Terwilliger, R. C. (1984) *Proc. Natl. Acad. Sci. U.S.A. 81*, 140–144.
Erickson, B. W., & Merrifield, R. B. (1976) in *The Proteins* (Neurath, H., & Hill, R. H., Eds.) Vol. II, pp 255–527, Academic Press, New York.
Garnier, J., Ogusthorpe, D. J., & Robson, B. (1978) *J. Mol. Biol. 120*, 97–120.
Gippert, G. P., Yip, P. F., Wright, P. E., & Case, D. A. (1990) *Biochem. Pharmacol. 40*, 15–22.
Goodman, M., Naider, F., & Toniolo, C. (1971) *Biopolymers 10*, 1719–1730.
Greff, D., Toma, F., Fermandjian, S., Löw, M., & Kisfaludy, L. (1976a) *Biochim. Biophys. Acta 439*, 219–231.
Greff, D., Fermandjian, S., Fromageot, P., Khosla, M. C., Smeby, R. R., & Bumpus, F. M. (1976b) *Eur. J. Biochem. 61*, 297–305.
Hodges, R. S., Burke, T. W. L., & Mant, C. T. (1988a) *J. Chromatogr. 444*, 349–362.
Hodges, R. S., Semchuk, P. D., Taneja, A. K., Kay, C. M., Parker, J. M. R., & Mant, C. T. (1988b) *Pept. Res. 1*, 19–30.
Hodges, R. S., Burke, T. W. L., & Mant, C. T. (1991) *J. Chromatogr. 548*, 267–280.
Jeener, J., Meier, B. H., Bachmann, P., & Ernst, R. R. (1979) *J. Chem. Phys. 71*, 4546–4553.
Jimenez, M. A., Nieto, J. L., Herranz, J., Rico, N., & Santoro, J. (1987) *FEBS Lett. 221*, 320–324.
Kabsch, W., Mannherz, H. G., Suck, D., Pai, E. F., & Holmes, K. C. (1990) *Nature 347*, 37–44.
Kim, P. S., & Baldwin, R. L. (1984) *Nature 307*, 329–334.
Kim, P. S., Bierzynski, A., & Baldwin, R. L. (1982) *J. Mol. Biol. 162*, 187–199.
Landis, C., & Allured, V. S. (1991) *J. Am. Chem. Soc. 113*, 9493–9499.
Lau, S. Y. M., Taneja, A. K., & Hodges, R. S. (1984a) *J. Biol. Chem. 259*, 13253–13621.
Lau, S. Y. M., Taneja, A. K., & Hodges, R. S. (1984b) *J. Chromatogr. 317*, 129–140.
Lehrman, S. R., Tuls, J. L., & Lund, M. (1990) *Biochemistry 29*, 5590–5596.
Leist, T., & Thomas, R. M. (1984) *Biochemistry 23*, 2541–2547.
Llinas, M., & Klein, M. P. (1975) *J. Am. Chem. Soc. 97*, 4731–4737.
Lu, Z. X., Fok, K. F., Erickson, B. W., & Hugli, T. E. (1984) *J. Biol. Chem. 259*, 7367–7370.
Mant, C. T., Burke, T. W. L., & Hodges, R. S. (1987) *Chromatographia 24*, 565–572.

Marion, D., Zasloff, M., & Bax, A. (1988) *FEBS Lett. 227*, 21–26.
Martenson, R. E., Park, J. Y., & Stone, A. L. (1985) *Biochemistry 24*, 7689–7695.
Maser, F., Bode, K., Pillai, V. N. R., & Mutter, M. (1984) *Adv. Polymer Sci. 65*, 179–213.
Moroder, L., Filippi, B., Borin, G., & Marchiori, F. (1975) *Biopolymers 14*, 2075–2093.
Mutter, M., & Altmann, K. H. (1985) *Int. J. Pept. Protein Res. 26*, 373–380.
Nelson, J. W., & Kallenbach, N. R. (1986) *Proteins 1*, 211–217.
Nelson, J. W., & Kallenbach, N. R. (1989) *Biochemistry 28*, 5256–5261.
Pastore, A., & Saudek, V. (1990) *J. Mag. Reson. 90*, 665–661.
Peña, M. C., Rico, M., Jimenez, M. A., Herranz, J., Santoro, J., & Nieto, J. L. (1989) *Biochim. Biophys. Acta 957*, 380–389.
Piantini, U., Sørensen, O. W., & Ernst, R. R. (1982) *J. Am. Chem. Soc. 104*, 6800–6801.
Rance, M., Sørensen, O. W., Bodenhausen, G., Wagner, G., Ernst, R. R., & Wüthrich, K. (1983) *Biochem. Biophys. Res. Commun. 117*, 479–485.
Reutimann, H., Straub, B., Luisi, P. L., & Holmgren, A. (1981) *J. Biol. Chem. 256*, 6796–6803.
Richardson, J. S., & Richardson, D. C. (1988) *Science 240*, 1648–1652.
Segawa, S. I., Fukuno, T., Fujiwara, K., & Noda, Y. (1991) *Biopolymers 31*, 491–509.
Siligardi, G., Drake, A. F., Mascagni, P., Neri, P., Lozzi, L., Niccolai, N., & Gibbons, W. A. (1987) *Biochem. Biophys. Res. Commun. 143*, 1005–1011.
Stone, A. L., Park, J. Y., & Martenson, R. E. (1985) *Biochemistry 24*, 6666–6673.
Tamburro, A. M., Scatturin, A., Rocchi, R., Marchiori, F., Borin, G., & Scoffone, E. (1968) *FEBS Lett. 1*, 298–300.
Torda, A. E., Scheek, R. M., & van Gunsteren, W. F. (1989) *Chem. Phys. Lett. 157*, 289–294.
Torda, A. E., Scheek, R. M., & van Gunsteren, W. F. (1990) *J. Mol. Biol. 214*, 223–235.
Van Eyk, J. E., & Hodges, R. S. (1991) *Biochemistry 30*, 11676–11682.
Van Eyk, J. E., Sönnichsen, F. D., Hodges, R. S., & Sykes, B. D. (1991) in *Peptides in Muscle Research* (Rüegg, J. C., Ed.) pp 15–31, Springer Verlag, Heidelberg.
Williams, R. W., Chang, A., Juretic, D., & Loughrams, S. (1987) *Biochem. Biophys. Acta 916*, 200–204.
Wishart, D. S., Sykes, B. D., & Richards, F. M. (1991) *J. Mol. Biol. 222*, 311–333.
Wüthrich, K. (1986) *NMR of Proteins and Nucleic Acids*, Wiley, New York.
Yamamoto, Y., Ohkubo, T., Kohara, A., Tanaka, T., Tanaka, T., & Kikuchi, M. (1990) *Biochemistry 29*, 8998–9006.
Zhou, N. E., Mant, C. T., & Hodges, R. S. (1990) *Peptide Res. 3*, 8–20.

Registry No. Actin 1–28, 137436-23-8; actin 1–20, 142948-04-7; actin 18–28, 142979-36-0; trifluoroethanol, 75-89-8.